31st Annual International Conference of the IEEE EMBS
Minneapolis, Minnesota, USA, September 2-6, 2009

Coarse-Grained Red Blood Cell Model with Accurate Mechanical Properties, Rheology and Dynamics

Dmitry A. Fedosov, Bruce Caswell, George E. Karniadakis

Abstract— **We present a coarse-grained red blood cell (RBC) model with accurate and realistic mechanical properties, rheology and dynamics. The modeled membrane is represented by a triangular mesh which incorporates shear inplane energy, bending energy, and area and volume conservation constraints. The macroscopic membrane elastic properties are imposed through semi-analytic theory, and are matched with those obtained in optical tweezers stretching experiments. Rheological measurements characterized by time-dependent complex modulus are extracted from the membrane thermal fluctuations, and compared with those obtained from the optical magnetic twisting cytometry results. The results allow us to define a meaningful characteristic time of the membrane. The dynamics of RBCs observed in shear flow suggests that a purely elastic model for the RBC membrane is not appropriate, and therefore a viscoelastic model is required. The set of proposed analyses and numerical tests can be used as a complete model testbed in order to calibrate the modeled viscoelastic membranes to accurately represent RBCs in health and disease.**

I. INTRODUCTION

Recent developments in sophisticated experimental techniques and instruments allow precise measurements of mechanical, rheological and dynamical properties of single cells. Examples are micropipette aspiration of a cell [1], cell deformation by optical tweezers [2], [3], optical magnetic twisting cytometry [4], three-dimensional measurement of cell membrane thermal fluctuations [5], and cells in shear flow [6]. These detailed experimental measurements provide a great potential for realistic numerical simulations of single cells and their suspensions (e.g., RBCs in health and disease, blood flow) by incorporating biologically relevant cell properties.

Distinct cell structures require a development of different models, however our focus will be primarily on accurate coarse-grained modeling of viscoelastic membranes, and in particular RBCs. The relative simplicity of RBC structure comprised of a membrane filled with a liquid cytosol of fixed volume makes it an excellent system for model development. The healthy RBC membrane has a biconcave shape of a diameter about 8 μm, and consists of a lipid bilayer with an attached cytoskeleton formed by spectrin protein network linked by short actin filaments. RBC can be considered to be a viscoelastic membrane taking into account the nearly viscous lipid bilayer and its area-incompressibility [7], while the attached elastic spectrin network is mainly responsible for the membrane integrity. A number of numerical RBC models have been developed recently [7], [8], [9], [10], [11], [12] representing a variety of methods. Most of the existing methods require extensive parameter calibration and focus on accurate incorporation of mechanical properties, which may limit their relevance in dynamics (e.g., blood flow). As an example, none of the models appear to consider the viscoelastic nature of the RBC membrane which affects RBC rheology and dynamics [4], [13].

We propose an accurate coarse-grained RBC model which addresses the issue of viscoelastic membrane modeling as a complex that includes cell mechanical properties, rheology and dynamics. Macroscopic membrane mechanical properties are imposed through a linear analysis avoiding any parameter calibration. We show how to effectively incorporate viscosity into the RBC membrane such that the numerical rheological measurements compare well with those derived from experiments [4]. In addition, RBC dynamics is verified against analytical predictions for a viscoelastic ellipsoid in shear flow [13]. These tests can be used as a complete test bed in order to incorporate realistic properties into the modeled viscoelastic membrane, which may accurately represent RBCs in health and disease and other types of cells of similar structure.

II. RED BLOOD CELL MODEL

The membrane model structure is defined by a set of points with Cartesian coordinates $\{\mathbf{x}_i\}$, $i \in 1...N_v$, that are vertices of a triangulated mesh on the surface. The vertices are connected by N_s springs, which form N_t triangles. The free energy of the system is given by

$$V(\{\mathbf{x}_i\}) = V_{inplane} + V_{bending} + V_{area} + V_{volume}. \qquad (1)$$

Here, the inplane energy mimics elastic properties of the underlying RBC spectrin network. The bending energy provides bending resistance of the lipid bilayer, while the area constraint enforces its area-incompressibility. The volume constraint is equivalent to incompressibility of the inner cytosol.

The inplane free energy term includes the springs energy as follows

$$V_{inplane} = \sum_{j \in 1...N_s} \left(\frac{k_B T l_m (3x_j^2 - 2x_j^3)}{4p(1-x_j)} + \frac{k_p}{(n-1) l_j^{n-1}} \right), \qquad (2)$$

where l_j is the length of the spring j, l_m is the maximum spring extension, $x_j = l_j / l_m$, $k_B T$ is the energy unit, p is the

Dmitry A. Fedosov is with the Division of Applied Mathematics, Brown University, Providence, RI 02912, USA (fedosov@dam.brown.edu)

Bruce Caswell is with Faculty of Division of Engineering, Brown University, Providence, RI 02912, USA (caswell@cfm.brown.edu)

George E. Karniadakis is with Faculty of Division of Applied Mathematics, Brown University, Providence, RI 02912, USA (gk@dam.brown.edu)

978-1-4244-3296-7/09/$25.00 ©2009 IEEE

persistence length, k_p is the spring constant, and n is a power. The first term in (2) corresponds to the attractive wormlike chain (WLC) potential, while the second term defines a repulsive force for $n > 0$ to be called the power force (POW), so that we abbreviate this spring model as WLC-POW. Note that if $n = 1$ the power force energy should be defined as $-k_p \log(l_j)$. A non-zero equilibrium spring length is defined by the balance of these two forces.

The bending energy is defined as

$$V_{bending} = \sum_{j \in 1...N_s} k_b \left[1 - cos(\theta_j - \theta_0)\right], \tag{3}$$

where k_b is the bending constant, θ_j is the instantaneous angle between two adjacent triangles having the common edge j and θ_0 is the spontaneous angle.

The area and volume conservation constraints are

$$V_{area} = \frac{k_a (A - A_0^{tot})^2}{2A_0^{tot}} + \sum_{j \in 1...N_t} \frac{k_d (A_j - A_0)^2}{2A_0}, \tag{4}$$

$$V_{volume} = \frac{k_v (V - V_0^{tot})^2}{2V_0^{tot}}, \tag{5}$$

where k_a, k_d and k_v are the global area, local area and volume constraint constants, respectively. The terms A and V are the total area and volume of RBC, while A_0^{tot} and V_0^{tot} are the desired total area and volume, respectively. Note that the second term in (4) corresponds to local area dilatation.

The forces exerted on each node are calculated from the above energies using the following expression

$$\mathbf{f}_i = -\partial V(\{\mathbf{x}_i\})/\partial \mathbf{x}_i, \qquad i \in 1...N_v. \tag{6}$$

This membrane model can be applied in many numerical methods. However, we employ Dissipative Particle Dynamics (DPD), a mesoscale method, for details see [14], [15].

III. RBC MECHANICS

A number of experiments to probe RBC mechanical properties were recently performed which include the micropipette aspiration technique [1] and RBC deformation by optical tweezers [2], [3]. The experimental shear modulus μ_0 is within the range of $2-15\ \mu N/m$ and the bending modulus k_c is between 1×10^{-19} and $7 \times 10^{-19}\ J$, which corresponds to the range of $23-163\ k_BT$ based on the normal body temperature $T = 36.6^oC$. Recent optical tweezers experiments [3] were quantified with the aid of continuum RBC modeling using a hyperelastic material model integrated by the finite element method (FEM). The membrane shear modulus of $\mu_0 = 8\ \mu N/m$ yielded the best fit to the experimental data which corresponds to the Young's modulus of $Y = 3\mu_0 = 24\ \mu N/m$.

A. Linear elastic and bending properties

Given an estimate of real elastic properties our goal is to specify the model parameters (e.g., spring, bending, area coefficients) such that the modeled membrane yields same mechanical properties. Linear analysis of small deformations is performed for a sheet of springs with regular hexagonal triangulation. Here, we correct and complete the analysis of [16]. Thus, the shear modulus μ_0 and the area-compression modulus K are expressed as

$$\mu_0 = \frac{\sqrt{3} k_B T x_0 (3 - x_0)}{16 p l_m (1 - x_0)^3} + \frac{\sqrt{3} k_p (n+1)}{4 l_0^{n+1}}, \tag{7}$$

$$K = 2\mu_0 + k_a + k_d, \tag{8}$$

where l_0 is the spring equilibrium length and $x_0 = l_0/l_m$. The above equations allow us to derive the model parameters for given macroscopic elastic properties. In addition, the bending coefficient k_b and the spontaneous angle θ_0 are given by

$$k_b = \frac{2}{\sqrt{3}} k_c, \qquad \theta_0 = cos^{-1}\left(\frac{\sqrt{3}(N_v - 2) - 5\pi}{\sqrt{3}(N_v - 2) - 3\pi}\right), \tag{9}$$

in relation to the bending rigidity k_c of the macroscopic model of Helfrich [17].

B. DPD units and scaling

The average equilibrium shape of a red blood cell measured in experiments [18] is biconcave given by the equation

$$z = \pm D_0 \sqrt{1 - \frac{4(x^2+y^2)}{D_0^2}} \left[a_0 + a_1 \frac{x^2+y^2}{D_0^2} + a_2 \frac{(x^2+y^2)^2}{D_0^4}\right], \tag{10}$$

where $D_0 = 7.82\ \mu m$ is the cell diameter, $a_0 = 0.05179025$, $a_1 = 2.002558$, and $a_2 = -4.491048$. The area and volume of this RBC is equal to 135 μm^2 and 94 μm^3, respectively. This shape is used for surface triangulation.

In order to relate DPD and real units we propose the following scaling. The length scale is based on the relation of modeled RBC diameter to the real diameter D_0 as

$$r_c = \frac{D_0^R}{D_0^D}[m], \tag{11}$$

where r_c is the DPD length scale, and superscripts R and D denote "real" and "DPD" units, respectively. The maximum spring extension is set to $l_m = 2.2 * l_0$, and this choice does not affect the linear elastic deformation, but it governs the RBC non-linear response at large deformation. Finally, we scale the energy units to correspond with Young's modulus as follows

$$(k_BT)^D = \frac{Y^R}{Y^D} \frac{r_c^2}{m^2} (k_BT)^R = \frac{Y^R}{Y^D} \left(\frac{D_0^R}{D_0^D}\right)^2 (k_BT)^R. \tag{12}$$

Note that for the stretching test we do not need to explicitly scale mass and time because here we are not interested in stretching dynamics.

C. RBC stretching test

A number of RBC stretching simulations were performed in order to validate our results against the experimental data of RBC deformation by optical tweezers [3]. The total stretching force lies in the range 0...200 pN, and is applied to 2% of vertices with the smallest x-coordinates in the negative x-direction and to 2% of vertices with the largest x-coordinates in the positive x-direction. The vertex

fraction of 2% corresponds to a contact diameter of the attached silica bead $d_c = 2\ \mu m$ used in experiments. Figure 1 presents RBC stretching response for different number of vertices N_v. An excellent agreement of the simulation

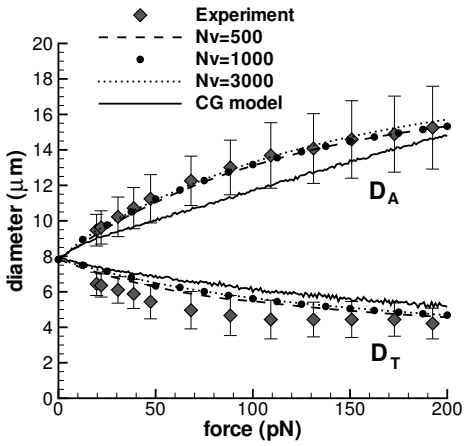

Fig. 1. Computational results for *different* N_v compared with the experiment [3] and coarse-grained RBC model (solid line) in [12]. D_A and D_T are axial and transverse RBC diameters, respectively.

results with the experiment is found for different coarse-graining levels (number of vertices). A small disagreement in the transverse diameter may result from rotation of the RBC in y-z plane in experiments (noticed in numerical simulations) which may lead to underprediction in D_T as the optical shape measurements were performed on a single observation angle. However, the simulation results remain within the experimental error bars. The solid line in figure 1 corresponds to the coarse-grained RBC model [12], however the estimation of linear elastic properties lacks a contribution of the area constraints, which results in Young's modulus underprediction of about 50%.

Despite the demonstrated success of the RBC model, it has several problems due to not having a stress-free membrane. The stretching deformation in different directions may give a distinct response, which worsens with more irregular triangulation compared with a plane hexagonal mesh. This makes the result dependent on triangulation quality. In addition, a slightly irregular mesh may require the bending rigidity to be set too high compared with the real one in order to maintain the equilibrium biconcave shape. Here, imposition of the real bending rigidity may result in relaxation to the stomatocyte (cup) shape, which is clearly an artifact of the model.

D. Stress-free membrane

In order to eliminate the aforementioned membrane stress artifacts we propose a simple modification to the described model. For each spring we define its equilibrium length l_0^i $i = 1...N_s$ which is obtained from the triangulation of the RBC equilibrium shape (10). Equation (7) is used to calculate the spring parameters p and k_p for the given shear modulus μ_0 based on the average spring length $\bar{l}_0 = \left(\sum_{i=1...N_s} l_0^i\right)/N_s$. Then, the persistence length p is kept constant for all springs, while the coefficient k_p is recalculated for every spring (define a set of k_p^i $i = 1...N_s$) based on the force balance $f_{WLC} = f_{POW}$ and the equilibrium spring length l_0^i. This sets the predefined equilibrium length to l_0^i for every spring and appears to accurately impose the specified shear modulus μ_0.

Figure 2 presents simulation results for a range of the number of vertices N_v from 100 to 27344. We find excellent

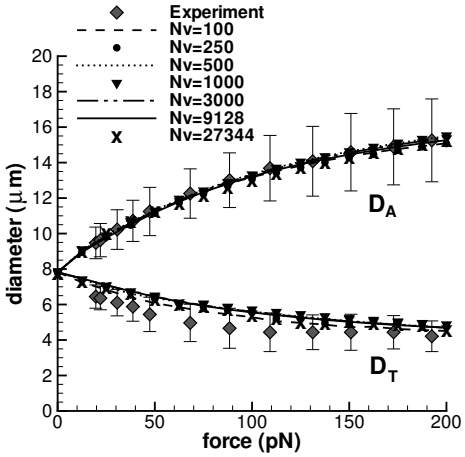

Fig. 2. Stress-free RBC model for different number of vertices compared with the experiment [3].

agreement of the numerical results with the experiment. Note that the stress-free model gives an identical stretching response when deformed along different directions. In addition, the deformation response is independent of triangulation. Here, $N_v = 27344$ corresponds to a spectrin-level of RBC modeling, while $N_v = 100 - 500$ is highly coarse-grained RBC. We suggest that the minimum N_v to be used for the RBC model should be about $250 - 300$ because a lower number of vertices may not provide a smooth RBC shape representation which could affect dynamics.

IV. RBC RHEOLOGY

Rheological measurements of the time-dependent complex modulus G^* were performed in experiments using optical magnetic twisting cytometry [4] showing the RBC membrane to be viscoelastic. In order to incorporate viscosity in the membrane model we introduce viscoelastic springs with a viscous contribution of $\xi \Delta v$, where ξ is the friction coefficient, and $\Delta v = v_1 - v_2$ is the velocity difference of the two ends. The modeled RBC is attached to the surface, and the mean square displacement (MSD) $< \Delta r^2(t) >$ of several points on its top is measured. Theoretical developments in microrheology [19] provide a relation between MSD and G^* as follows

$$G^*_{2D}(\omega) = \frac{k_B T}{< \Delta r^2(t_\infty) > + i\omega < \Delta r^2(\omega) >}, \qquad (13)$$

where $i = \sqrt{-1}$, and $< \Delta r^2(\omega) >$ is the unilateral Fourier transform of $< \Delta r^2(t) > - < \Delta r^2(t_\infty) >$. Figure 3 shows the storage g' and the loss g'' moduli results. Here, the scaling in vertical axes is performed according to the scaling defined

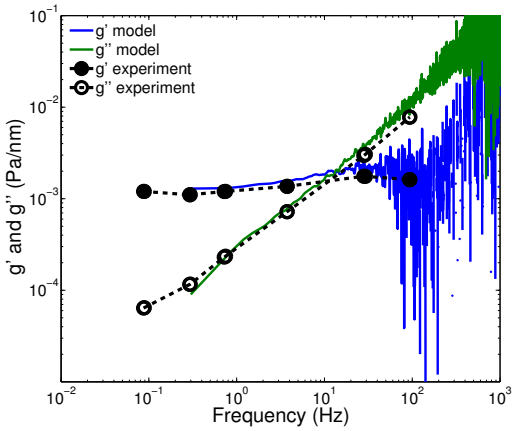

Fig. 3. Storage g' and loss g'' moduli results compared with the experiment [4].

above as $g'^{D}(k_BT)^D/r_c^4 = g'^{R}Pa/nm$. The scaling in time or frequency is done according to a characteristic time t_c defined by intersection of g' and g''. We showed that the time t_c can be uniquely related to the membrane elastic properties and total viscous dissipation (fluid and membrane viscosity contributions), which defines meaningful characteristic time scale. Note that the scatter at high frequencies is due to data underresolution at short times.

V. RBC DYNAMICS

While the behavior of fluid membranes in flow is reasonably well studied experimentally, analytically and numerically, the dynamics of viscoelastic membranes is not well understood. Recent analytical results for viscoelastic ellipsoids in shear flow [13] suggest that the dynamics of such membranes is governed by membrane geometry, elastic properties, the ratio of membrane to fluid viscosity λ, and flow conditions. This theory applied to red blood cells suggests that there exists three characteristic regions of RBC dynamics in shear flow depending on λ and shear rate: (i) solid-like *tumbling* motion, (ii) stable *tank-treading*, and (iii) *intermittent* which can be considered as an unstable behavior combining two previous motions in a sequence. If λ is smaller than about 2.5 there exists a characteristic shear rate range (relatively narrow) where the RBC is subject to intermittent behavior, and for shear rates below that range the RBC tumbles, and tank-treads for shear rates above the range. However, if λ is greater than 2.5 (as for real RBCs in blood plasma) only two regions are defined, tumbling at low shear rates and intermittent for higher shear rates. We performed a number of simulations of RBC dynamics in shear flow in order to compare the results with the aforementioned analytical predictions. We were able to qualitatively reproduce RBC dynamics characterized by the described behavior. In our ongoing work we attempt to make a connection between the time scale t_c and the shear rate in flow in order to obtain quantitative agreement.

VI. CONCLUSIONS

We presented a general coarse-grained RBC model built as a network of springs in combination with bending rigidity, area and volume conservation constraints. The model accurately captures elastic response at small and large deformations for different levels of coarse-graining. The RBC is modeled as viscoelastic membrane which yields accurate rheological properties and dynamics. This model can be used for simulations of RBCs in health and disease, and other cells having a viscoelastic membrane structure.

VII. ACKNOWLEDGMENTS

This work was supported by NSF grants OCI and CI-Team.

REFERENCES

[1] D.E. Discher, N. Mohandas, E.A. Evans, Molecular maps of red cell deformation: hidden elasticity and in situ connectivity, *Science*, vol. 266, 1994, pp 1032-1035.
[2] M. Dao, C.T. Lim, S. Suresh, Mechanics of the human red blood cell deformed by optical tweezers, *J. Mech. Phys. Solids*, vol. 51, 2003, pp 2259-2280.
[3] J.P. Mills, L. Qie, M. Dao, C.T. Lim, S. Suresh, Nonlinear elastic and viscoelastic deformation of the human red blood cell with optical tweezers, *Mech. Chem. Biosys.*, vol. 1, 2004, pp 169-180.
[4] M. Puig-de-Morales-Marinkovic, K.T. Turner, J.P. Butler, J.J. Fredberg, S. Suresh, Viscoelasticity of the human red blood cell, *Am. J. Physiol.: Cell Physiol.*, vol. 293, 2007, pp 597-605.
[5] Y.K. Park, M. Diez-Silva, G. Popescu, G. Lykotrafitis, W. Choi, M.S. Feld, S. Suresh, Refractive index maps and membrane dynamics of human red blood cells parasitized by Plasmodium falciparum, *Proc. Nat. Acad. Sci. USA*, vol. 105, 2008, pp 13730-13735.
[6] T.M. Fischer, Shape memory of human red blood cells, *Biophys. J.*, vol. 86, 2004, pp 3304-3313.
[7] Y.C. Fung, *Biomechanics: Mechanical properties of living tissues*, 2nd ed., Springer-Verlag, NY, 1993.
[8] C. Pozrikidis, Numerical Simulation of Cell Motion in Tube Flow, *Ann. Biomed. Engin.*, vol. 33, 2005, pp 165-178.
[9] D.E. Discher, D.H. Boal, S.K. Boey, Simulations of the erythrocyte cytoskeleton at large deformation. II. Micropipette aspiration, *Biophys. J.*, vol. 75, 1998, pp 1584-1597.
[10] H. Noguchi, G. Gompper, Shape transitions of fluid vesicles and red blood cells in capillary flows, *Proc. Nat. Acad. Sci. USA*, vol. 102, 2005, pp 14159-14164.
[11] M.M Dupin, I. Halliday, C.M. Care, L. Alboul, L.L. Munn, Modeling the flow of dense suspensions of deformable particles in three dimensions, *Phys. Rev. E*, vol. 75, 2007, pp 066707.
[12] I.V. Pivkin and G.E. Karniadakis, Accurate coarse-grained modeling of red blood cells, *Phys. Rev. Lett.*, vol. 101, 2008, pp 118105.
[13] J.M Skotheim, T.W. Secomb, Red blood cells and other nonspherical capsules in shear flow: Oscillatory dynamics and the tank-treading-to-tumbling transition, *Phys. Rev. Lett.*, vol. 98, 2007, pp 078301.
[14] P.J. Hoogerbrugge and J.M.V.A. Koelman, Simulating microscopic hydrodynamic phenomena with dissipative particle dynamics, *Europhys. Lett.*, vol. 19, 1992, pp 155-160.
[15] R.G. Groot and P.B. Warren, Dissipative particle dynamics: Bridging the gap between atomistic and mesoscopic simulation, *J. Chem. Phys.*, vol. 107, 1997, pp 4423-4435.
[16] M. Dao, J. Li, S. Suresh, Molecularly based analysis of deformation of spectrin network and human erythrocyte, *Mater. Sci. Engin. C*, vol. 26, 2006, pp 1232-1244.
[17] W. Helfrich, Elastic properties of lipid bilayers: theory and possible experiments, *Z Naturforsch C*, vol. 28, 1973, pp 693-703.
[18] E.A. Evans and R. Skalak, *Mechanics and thermodynamics of biomembranes*, CRC Press, Inc., Boca Raton, FL; 1993.
[19] E. Helfer, S. Harlepp, L. Bourdieu, J. Robert, F.C. MacKintosh, D. Chatenay, Microrheology of biopolymer-membrane complexes, *Phys. Rev. Lett.*, vol. 85, 2000, pp 457-460.